Journal of Power Sources 194 (2009) 338–348

Contents lists available at ScienceDirect

Journal of Power Sources

journal homepage: www.elsevier.com/locate/jpowsour

Nonlinear robust control of proton exchange membrane fuel cell by state feedback exact linearization

Q. Li [a,*], W. Chen [a], Y. Wang [b], J. Jia [b], M. Han [c]

[a] School of Electrical Engineering, Southwest Jiaotong University, Chengdu 610031, Sichuan Province, China
[b] School of Electrical & Electronic Engineering, Nanyang Technological University, Nanyang Avenue 639798, Singapore, Singapore
[c] School of Engineering, Temasek Polytechnic, Tampines 529757, Singapore, Singapore

ARTICLE INFO

Article history:
Received 9 March 2009
Received in revised form 28 April 2009
Accepted 30 April 2009
Available online 9 May 2009

Keywords:
Proton exchange membrane fuel cell
Dynamic nonlinear model
State feedback exact linearization
Dynamic extension algorithm
H_∞ robust control

ABSTRACT

By utilizing the state feedback exact linearization approach, a nonlinear robust control strategy is designed based on a multiple-input multiple-output (MIMO) dynamic nonlinear model of proton exchange membrane fuel cell (PEMFC). The state feedback exact linearization approach can achieve the global exact linearization via the nonlinear coordinate transformation and the dynamic extension algorithm such that H_∞ robust control strategy can be directly utilized to guarantee the robustness of the system. The proposed dynamic nonlinear model is tested by comparing the simulation results with the experimental data in Fuel Cell Application Centre in Temasek Polytechnic. The comprehensive results of simulation manifest that the dynamic nonlinear model with nonlinear robust control law has better transient and robust stability when the vehicle running process is simulated. The proposed nonlinear robust controller will be very useful to protect the membrane damage by keeping the pressure deviations as small as possible during large disturbances and prolong the stack life of PEMFC.

© 2009 Elsevier B.V. All rights reserved.

1. Introduction

As a renewable energy source, fuel cells are one of the promising energy technologies for sustainable future due to their high energy efficiency and environment friendliness. Compared with the other types of fuel cells, a proton exchange membrane fuel cell (PEMFC) shows promising results with its advantages such as low temperature, high power density, fast response, and zero emission if it is run with pure hydrogen, and it is suitable for use in portable power supply, vehicles, and residential and distributed power plants [1–3].

PEMFC is a nonlinear, multiple-input and output, and strongly coupled dynamic system. Its working process is accompanied with liquid/vapor/gas mixed flow transportation, heat conduction and electrochemical reaction. The output current changes when the drove load changes, and electrochemical reaction is accelerated, simultaneously. If the flow rate of oxygen is too low in cathode, the output power of PEMFC system could be decreased because of lacking oxygen, which is so-called starvation. Therefore, in order to generate a reliable and efficient power response and prevent membrane damage as well as detrimental degradation of the stack voltage and oxygen depletion, it is so significant to design an effective control scheme to achieve optimal air and hydrogen inlet flow rates.

At present, many control strategies have been adopted for controlling the PEMFC system. Vahidia et al. [4] adopted a predicting control method to design the controller for fuel cell vehicle and it could satisfy the quickness response of air supply. Golbert and Lewind [5] who made fuel cell model linearization used predicting control to satisfy the need of power. Yuan et al. [6] imposed a predicting control method based on support vector machine to fuel cell control system. Schumacher et al. [7] proposed a water management of PEMFC method using fuzzy control. According to the experimental data, Almeda and Smoesm [8] proposed an artificial neural network control method to control output voltage of fuel cell and optimize the parameters in the system. Pukrushpan co-workers [9,10] used feed-forward and feedback strategies to control the flow rate of compressor in the PEMFC air supply system. However, the existing control approaches used for PEMFC were based on linear models which were linearized at a specific operating point. Chiu et al. [11] proposed a linear PEMFC models which was used Jacobian linearization via a Taylor series expansion at the nominal operating point. However, the proposed model could not easily achieve satisfactory dynamic performance under large disturbances because of the operational parametric uncertainties such as the uncertainties of parametric coefficients for each cell on kinetic, thermodynamic and electrochemical foundations, and the resistivity of the membrane for the electron flow. Na co-workers [12,13] presented a nonlinear controller which was designed based on the nonlinear model to prolong the stack life of fuel cells. The simulation results showed that the proposed nonlinear controls had better transient

* Corresponding author.
E-mail address: liqi0800@gmail.com (Q. Li).

0378-7753/$ – see front matter © 2009 Elsevier B.V. All rights reserved.
doi:10.1016/j.jpowsour.2009.04.077

performances than the linear controls. However, the feedback linearization approach was used to only achieve the local linearization without the nonlinear coordinate transformation because of lacking the relative degree of the system. The proposed nonlinear controller could not guarantee the robustness with the operational parametric uncertainties and the internal dynamics problem would be appeared out. Therefore, an accurate nonlinear dynamic model needs to be developed for PEMFC as well as an advanced controller design technique, considering the nonlinearity and uncertainty that need to be proposed.

Recently, the state feedback exact linearization for nonlinear dynamic models, a well-known nonlinear approach, has been widely used to achieve more robust transient behavior [14,16,17]. The state feedback exact linearization uses a nonlinear transformation to transform an original nonlinear dynamic model into a linear model by diffeomorphism mapping. An optimal control theory is also applied to obtain a linear control that is transformed back to the original space by using the nonlinear mapping. The purpose of the dynamic extension algorithm is to construct an extended system in which the relative degree is equal to the order of the system [15]. After using the dynamic extension algorithm, the internal dynamics problem can be avoided and the nonlinear system becomes global linearized via the state feedback exact linearization.

H_∞ control approach has a broad base of support because of its robustness to uncertainties and reliable design algorithms [18–20]. The weighting functions chosen to shape the sensitivity functions are obtained through analysis of the uncertainties present in the system as well as from frequency-domain and time-domain requirements. Therefore, in the framework of H_∞ mixed sensitivity design, the nonlinear H_∞ robust control based on the state feedback exact linearization could make the system possess better robust stability.

In this paper, a MIMO dynamic nonlinear model that is appropriate for developing a nonlinear robust controller is proposed. The state feedback exact linearization with the dynamic extension algorithm is applied to design the proposed robust controller, based directly on the nonlinear dynamic PEMFC model. The dynamic response of the proposed model is tested by fuel cell test system. The control law obtained from the state feedback exact linearization is expected to be more robust in the presence of large disturbances when the vehicle running process is simulated. Furthermore, PEMFC life can be prolonged and protected by minimizing the deviations between the hydrogen and oxygen partial pressures.

2. The modeling of PEMFC

2.1. The theory of PEMFC

The fuel cell is an electrochemical energy device that converts the chemical energy of fuel directly into electricity and heat with water as a byproduct of the reaction. The hydrogen and oxygen work as fuel and oxidant and they need to be humidified before they are fed into the cell/stack. The positively charged protons diffuse from anode through one side of the membrane and migrate toward the cathode [21–24]. The electrons pass from the anode to the cathode through an exterior circuit and provide electric power along the way; the byproduct water will be drained out with the gases. The work process and reaction principle are shown in Fig. 1.

In order to simplify the analysis, several assumptions are made as below:

(1) The stack is well designed so that all cells perform similarly and can be lumped as a stack.
(2) All gases obey the ideal gas law and are equably distributed.

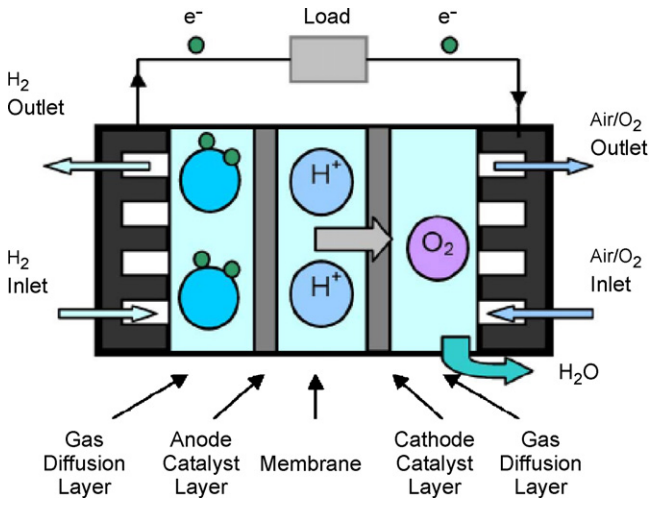

Fig. 1. The work process and reaction principle of the PEM fuel cell.

(3) Due to a slow response time regarding the stack temperature, the operating stack temperature is assumed to be constant.
(4) The temperature of hydrogen inside the anode and oxygen inside the cathode are equal to the stack temperature.
(5) For water management, it is assumed that the liquid water evaporates into the cathode or anode gas if humidity on either side drops below 100%.
(6) It is assumed that pure hydrogen (99.99%) is fed to the anode, and air that is uniformly mixed with nitrogen and oxygen by a ratio of 21:79 is supplied to the cathode.

2.2. The output voltage model

The ideal standard potential of a hydrogen/oxygen fuel cell which is obtained for standard state conditions (25 °C and 1 atm) is 1.229 V with liquid water product. However, the actual cell potential is decreased from its equilibrium potential because of irreversible losses. There are three types of the irreversible losses, namely activation losses, ohmic losses and concentration losses. At low current densities, the activation losses of oxygen reduction reaction are almost entirely responsible for the potential drop of the cell; at the high current densities, the concentration losses become more significant. The output voltage of the single cell is given by Eq. (1) according to the PEMFC output characteristics empirical equation which is developed by Amphlett et al. [24] and Kim et al. [25],

$$U_{\text{cell}} = E_{\text{Nernst}} - U_{\text{act}} - U_{\text{ohmic}} - U_{\text{con}} \quad (1)$$

where E_{Nernst} is thermodynamic potential, U_{act} is activation losses, U_{ohmic} is ohmic losses, U_{con} is concentration loss.

$$E_{\text{Nernst}} = \frac{1}{2F}\left[\Delta G - \Delta S(T - T_{\text{ref}}) + RT(\ln P_{\text{H}_2} + \frac{\ln P_{\text{O}_2}}{2})\right] \quad (2)$$

where ΔG is Gibb's free energy change, ΔS is standard mole entropy change, R is gaseous constant, F is Faraday's constant, T_{ref} is reference temperature, P_{H_2} is partial pressure of hydrogen, P_{O_2} is partial pressure of oxygen.

The activation loss of PEMFC is caused by the sluggish kinetics of the reactions taking place on the active surface of electrodes [26,28].

$$U_{\text{act}} = \xi_1 + \xi_2 T + \xi_3 T(\ln \text{CO}) + \xi_4 T(\ln I_{\text{s}}) \quad (3)$$

where I_{st} is the load current of PEMFC, ξ_1, ξ_2, ξ_3, ξ_4 are the model coefficient got by experimental data fitting based on electrochemistry, thermodynamics and fluid mechanics, CO_2 is dissolved oxygen concentration in the interface of the cathode catalyst.

According to the definition of Henry's law [27], it yields,

$$CO_2 = \frac{P_{O_2}}{5.08 \times 10^6 \exp(-498/T)} \tag{4}$$

Different from the ohmic losses empirical equation which is already presented, in this model ohmic losses consist of the voltage drop which is caused by R_M, the equivalent membrane impedance and the voltage drop that is caused by R_c, the contact resistances both between the membrane and electrodes as well as the electrodes and the bipolar plates which is constant once the cell is fabricated [27,28].

$$U_{ohmic} = I_{st}(R_M + R_c) \tag{5}$$

$$R_M = \frac{r_M l}{A_{fc}} \tag{6}$$

where l is the thickness of the membrane, A_{fc} is the cell active area. The resistivity r_M of Nafion series proton exchanging membrane can be calculated by Eq. (7) [27].

$$r_M = \frac{181.6[1 + 0.03(I_{st}/A_{fc}) + 0.062(T/303)^2(I_{st}/A_{fc})^{2.5}]}{[\lambda - 0.634 - 3(I_{st}/A_{fc})]\exp[4.18(T - 303/T)]} \tag{7}$$

where λ is the water content of the membrane.

Concentration losses are caused by the mass transportation which in turn affects the concentration of the hydrogen and oxygen at high current density [28,30].

$$U_{con} = B \ln\left(1 - \frac{i_{st}}{i_{max}}\right) \tag{8}$$

where B is determined by the PEMFC and its working status, i_{st} is the current density of fuel cell, i_{max} is maximum current density.

There exists charge double layer in the PEMFC, Larminie et al. [1] and Wang et al. [30] analyzed the charge double layer at the surface of the cathode. The equivalent capacitance C can smooth the voltage drop effectively. As the function of the charge double layer, the PEMFC bears eminent dynamic characteristics. If u_d is the overall voltage drop, the dynamic characteristics of the single cell can be expressed in the differential Eq. (9), which is distinct from the steady-state model.

$$\frac{du_d}{dt} = \frac{I_{st}}{C} - \frac{u_d}{\tau} \tag{9}$$

where the time constant τ will change with the load changing, which will affect the dynamic response of the voltage as shown in Eq. (10).

$$\tau = C\left(\frac{U_{act} + U_{con}}{I_{st}}\right) \tag{10}$$

Considering synthetically the thermal characteristic, momentum characteristic and the mass transportation, the output voltage of PEMFC can be expressed as Eq. (11).

$$U_{cell} = E_{Nersnt} - U_{ohmic} - u_d \tag{11}$$

2.3. The anode pressure model

According to the ideal gas law and the mode conservation rule, the partial pressure of each gas is balanced by the gas inlet flow rate minus the gas consumption and the gas outlet flow rate. The partial pressure derivatives are given as follows [29,31,32].

Anode mole conservation:

$$\frac{dP_{H_2}}{dt} = \frac{RT}{V_a}(W_{H_2,in} - W_{H_2,purge} - W_{H_2,ret}) \tag{12}$$

$$\frac{dP_{w,an}}{dt} = \frac{RT}{V_a}(W_{v,an,in} - W_{v,an,purge} - W_{v,mbr}) \tag{13}$$

where P_{H_2} and $P_{w,an}$ are the partial pressure of hydrogen and water in the anode respectively, $W_{H_2,in}$ is the inlet mass flow rate of hydrogen, $W_{H_2,purge}$ is the hydrogen mass flow rate purged out the anode, $W_{H_2,ret}$ is the reacted mass flow rate of hydrogen, $W_{v,an,in}$ is the water mass flow rate into the anode, $W_{v,an,purge}$ is the purged water mass flow rate, $W_{v,mbr}$ is the water flow rate across the membrane.

With the measured inlet flow rates and the stack current, the outlet flow rates are given by A_{in} which is the summations of anode inlet flow rates minus the reacted gas.

$$W_{H_2,ret} = N\frac{A_{fc} i_{st}}{2F} = Q_1 i_{st} \tag{14}$$

$$W_{H_2,purge} = (A_{in} - Q_1 i_{st})F_{H_2} \tag{15}$$

$$W_{H_2,in} = Y_{H_2} A_{in} \tag{16}$$

$$F_{H_2} = \frac{P_{H_2}}{P_{H_2} + P_{w,an}} \tag{17}$$

$$A_{in} = s_{H_2} u_a k_a \tag{18}$$

where N is the cell number Y_{H_2} is the mole fractions of hydrogen, F_{H_2} is the pressure fraction of hydrogen inside the anode, u_a is the input control variable of anode, k_a is the conversion factors of anode, S_{H_2} is hydrogen stoichiometry.

The membrane hydration model captures the effect of water transport across the membrane. Both water content and mass flow are assumed to be uniform over the surface area of the membrane [31,32]. The water inlet flow rates on the anode and the cathode are expressed in terms of the relative humidity, saturation pressure, and total pressure on each side.

$$W_{v,mbr} = NM_v A_{fc} n_d \frac{i_{st}}{F} = Q_2 i_{st} \tag{19}$$

$$W_{v,an,purge} = (A_{in} - Q_2 i_{st})F_{v,an} \tag{20}$$

$$W_{v,an,in} = \frac{\varphi_a P_v}{P_{H_2} + P_{w,an} - \varphi_a P_v} A_{in} \tag{21}$$

$$F_{v,an} = \frac{P_{w,an}}{P_{H_2} + P_{w,an}} \tag{22}$$

$$\log_{10}(P_v) = -1.69 \times 10^{-10} T^4 + 3.85 \times 10^{-7} T^3 - 3.39 \times 10^{-4} T^2 + 0.143T - 20.92 \tag{23}$$

where n_d is the electro-osmotic drag coefficient, M_v is the vapor molar mass, φ_a is the relative humidity in the anode, P_v is the saturation pressure.

2.4. The cathode pressure model

This model captures the cathode air flow behavior. Cathode mole conservation [29,31,32]:

$$\frac{dP_{O_2}}{dt} = \frac{RT}{V_c}(W_{O_2,in} - W_{O_2,out} - W_{O_2,ret}) \tag{24}$$

$$\frac{dP_{N_2}}{dt} = \frac{RT}{V_c}(W_{N_2,in} - W_{N_2,out}) \tag{25}$$

$$\frac{dP_{w,ca}}{dt} = \frac{RT}{V_c}(W_{v,ca,in} - W_{v,ca,out} + W_{v,gen} + W_{v,mbr}) \tag{26}$$

where P_{O_2}, P_{N_2} and $P_{w,ca}$ are the partial pressure of oxygen, nitrogen and water in the cathode respectively, $W_{O_2,in}$ and $W_{N_2,in}$ are the oxygen mass flow rate and the nitrogen mass flow rate into the cathode respectively, $W_{O_2,ret}$ is the reacted oxygen mass flow rate in the cathode, $W_{O_2,out}$ and $W_{N_2,out}$ are the oxygen mass flow rate and the nitrogen mass flow rate out the cathode respectively, $W_{v,gen}$ is

the reacted water mass flow rate, $W_{v,ca,in}$ and $W_{v,ca,out}$ are the water mass flow rate into the cathode and out the cathode ,respectively.

$$W_{O_2,ret} = N\frac{A_{fc}i_{st}}{4F} = i_{st}\frac{Q_1}{2} \tag{27}$$

$$W_{O_2,out} = \left(C_{in} - i_{st}\frac{Q_1}{2}\right)F_{O_2} \tag{28}$$

$$W_{N_2,out} = C_{in}F_{N_2} \tag{29}$$

$$W_{O_2,in} = Y_{O_2}C_{in} \tag{30}$$

$$W_{N_2,in} = Y_{N_2}C_{in} \tag{31}$$

$$F_{O_2} = \frac{P_{O_2}}{P_{O_2} + P_{N_2} + P_{w,ca}} \tag{32}$$

$$F_{N_2} = \frac{P_{N_2}}{P_{O_2} + P_{N_2} + P_{w,ca}} \tag{33}$$

$$C_{in} = s_{air}u_c k_c \tag{34}$$

where C_{in} is the summations of cathode inlet flow rates, Y_{O_2} and Y_{N_2} are the mole fractions of oxygen and nitrogen, F_{O_2} and F_{N_2} are the pressure fraction of oxygen and nitrogen inside the cathode, u_c is the input control variable of cathode, k_c is the conversion factors of cathode, s_{air} is air stoichiometry.

$$W_{v,ca,out} = (C_{in} - Q_2 i_{st})F_{v,ca} \tag{35}$$

$$W_{v,ca,in} = \frac{\varphi_c P_v}{P_{O_2} + P_{w,ca} - \varphi_c P_v}C_{in} \tag{36}$$

$$W_{v,gen} = N\frac{A_{fc}i_{st}}{2F} = Q_1 i_{st} \tag{37}$$

$$F_{v,ca} = \frac{P_{w,ca}}{P_{O_2} + P_{N_2} + P_{w,ca}} \tag{38}$$

where φ_c is the relative humidity in the cathode.

In addition, if the mass of water calculated is greater than the maximum mass of vapor, the liquid water formation occurs simultaneously. The flow rates of liquid water leaving the anode and cathode are dependent upon the saturation state of each gas [10]. The mass of liquid water and vapor is calculated as follows:

if $m_{w,an\,or\,ca} \le m_{v,max,an\,or\,ca} \rightarrow m_{v,an\,or\,ca} = m_{w,an\,or\,ca}, \quad m_{1,an\,or\,ca} = 0;$

if $m_{w,an\,or\,ca} > m_{v,max\,an\,or\,ca} \rightarrow m_{v,an\,or\,ca} = m_{w,max,an\,or\,ca},$

$m_{1,an\,or\,ca} = m_{w,an\,or\,ca} - m_{w,max,an\,or\,ca}.$

In designing PEMFC control, the main focus is on the control of hydrogen and oxygen partial pressures, which can avoid unwanted pressure fluctuation and prevent the membrane electrode assemblies (MEAs) from collapsing by minimizing the pressure difference between the anode and the cathode.

3. Nonlinear control by state feedback exact linearization

For chemical process control, nonlinear control theory developed from differential geometry, known as exact linearization or feedback linearization, has more attractive because many chemical processes are basically of high nonlinearity [31,33]. Hence, one of the main motivations of utilizing state feedback exact linearization for a PEMFC system is inherently a nonlinear chemical process.

3.1. State feedback exact linearization

The objective of state feedback exact linearization is to create a linear differential relation between the output y and a newly defined input v. The notation and concepts of differential geometry are essential to understand this approach. Consider a MIMO nonlinear system

$$\begin{aligned} \dot{x} &= f(x) + \sum_{i=1}^{m} g_i(x)u_i \\ y_i &= h_i(x), \qquad i = 1, 2, \ldots, m \end{aligned} \tag{39}$$

where x is an n-dimensional state vector that is assumed to be measurable, u and y are m-dimensional input and output vectors.

The *Lie* derivative of a scalar function $h(x)$ with respect to a vector function $f(x)$ is defined as

$$L_f h(x) = \nabla h f = \frac{\partial h(x)}{\partial x}f(x) \tag{40}$$

Repeated *Lie* derivatives can be defined recursively as

$$\begin{aligned} L_f^k h(x) &= L_f(L_f^{k-1}h) = \nabla(L_f^{k-1}h)f \\ L_f^0 h(x) &= h(x) \qquad\qquad k = 1, 2, \ldots \end{aligned} \tag{41}$$

Similarly, in the case of another vector field g

$$L_g L_f h(x) = \nabla(L_f h)g \tag{42}$$

The output needs to be differentiated for r times until it is directly related to the input u. The number r is called the relative degree of the system. The MIMO system is said to have a vector relative degree $\{r_1, r_2, \ldots, r_m\}$ at a point x_0 if

(1) $L_{gj}L_f^k h_i(x) = 0$ for all $1 \le j \le m$, all $1 \le i \le m$, $k < r_i - 1$, and for all x in the neighborhood of x_0;
(2) $m \times m$ matrix

$$E(x) = \begin{bmatrix} L_{g_1}L_f^{r_1-1}h_1(x) & \cdots & L_{g_m}L_f^{r_1-1}h_1(x) \\ \vdots & \cdots & \vdots \\ L_{g_1}L_f^{r_m-1}h_m(x) & \cdots & L_{gm}L_f^{r_m-1}h_m(x) \end{bmatrix} \tag{43}$$

is nonsingular at $x = x_0$, which is called as a decoupling matrix. If $E(x)$ is singular, a considerably more elaborate analysis is required.

Considering a nonlinear system has the relative degree $r_1 + r_2 + \cdots + r_m = n$, a nonlinear coordinate transformation in the state space is defined as

$$z_k^i = \Phi^i(x) = \begin{bmatrix} \phi_1^i(x) \\ \phi_2^i(x) \\ \cdots \\ \phi_k^i(x) \end{bmatrix} = \begin{bmatrix} h_i(x) \\ L_f h_i(x) \\ \cdots \\ L_f^{k-1}h_i(x) \end{bmatrix}, \quad 1 \le i \le m, 1 \le k \le r_i \tag{44}$$

where is called a local diffeomorphism, in which the map between the new input v and the output is exactly linear for all x in the neighborhood of x_0. Then there exists a nonlinear static feedback such that the closed-loop system in the new coordinates is linear and controllable.

In the new coordinates the system is given

$$\begin{aligned} &\dot{z}_1^i = z_2^i, \qquad 1 \le i \le m \\ &\vdots \\ &\text{by } \dot{z}_{r_i-1}^i = z_{r_i}^i, \qquad 1 \le i \le m \text{ where} \\ &\dot{z}_{r_i}^i = b_i(z) + \sum_{j=1}^{m} a_{ij}(z)u_j, \quad 1 \le i \le m \end{aligned}$$

$$b_i(z) = L_f^{r_i}h_i(\phi^{-1}(z)) \quad a_{ij}(z) = L_{g_j}L_f^{r_i-1}h_i(\phi^{-1}(z))$$

Suppose that the matrix $z_{r_i}^i$ $(1 \le i \le m)$ is

$$\begin{bmatrix} \dot{z}_{r_1}^1 \\ \vdots \\ \dot{z}_{r_m}^m \end{bmatrix} = b(z) + E(z)u = \begin{bmatrix} b_1(z) \\ \vdots \\ b_m(z) \end{bmatrix} + \begin{bmatrix} a_{11}(z) & \cdots & a_{1m}(z) \\ \vdots & \cdots & \vdots \\ a_{m1}(z) & \cdots & a_{mm}(z) \end{bmatrix} \begin{bmatrix} u_1 \\ \vdots \\ u_m \end{bmatrix} \tag{46}$$

Then a newly vector input is defined based on above the matrix

$$b(z) + E(z)u = v = \begin{bmatrix} v_1 \\ \vdots \\ v_m \end{bmatrix} = \begin{bmatrix} y_1^{(r_1)} \\ \vdots \\ y_m^{(r_m)} \end{bmatrix} \tag{47}$$

Therefore the state feedback control law of the MIMO nonlinear system is defined as

$$u = -E^{-1}(z)b(z) + E^{-1}(z)v \tag{48}$$

Note that the control law in Eq. (48) transforms the nonlinear system into a linear one in which the aforementioned input–output relation is linearized and decoupled.

The resulting closed-loop system which is so-called Brunovsky canonical form is then governed by the equations

$$\begin{aligned} &\dot{z}_1^i = z_2^i, && 1 \le i \le m \\ &\vdots \\ &\dot{z}_{r_i-1}^i = z_{r_i}^i, && 1 \le i \le m \\ &\dot{z}_{r_i}^i = v_i, && 1 \le i \le m \end{aligned} \tag{49}$$

Above the coordinates transformation and state feedback problems are so-called state feedback exact linearization problem. Then the new linear state-space equation is

$$\dot{z}_{r_i}^i = A_i z_{r_i}^i + B_i v_i, \quad 1 \le i \le m \tag{50}$$

with

$$A_i = \begin{bmatrix} 0 & 1 & 0 & \cdots & 0 \\ 0 & 0 & 1 & \cdots & 0 \\ \vdots & \vdots & \vdots & \vdots & \vdots \\ 0 & 0 & 0 & \cdots & 1 \\ 0 & 0 & 0 & 0 & 0 \end{bmatrix}_{m \times m} \quad B_i = \begin{bmatrix} 0 \\ 0 \\ 0 \\ \vdots \\ 1 \end{bmatrix}_{m \times 1}$$

The matrix A_i and the vector B_i satisfy the controllable condition.

$$\operatorname{rank}(B_i\ A_iB_i \ldots A_i^{n-1}B_i) = n$$

In this paper, the state feedback exact linearization is utilized according to the MIMO dynamic nonlinear model of the PEMFC.

3.2. Dynamic extension algorithm

To apply the state feedback exact linearization, the relative degree vector has to be checked such that the internal dynamics problem is avoided. Without solving the internal dynamics issue, the nonlinear controller would be practically meaningless because the instability of the internal dynamics causes undesirable phenomena such as a poor response and critical damage to the system. Therefore, the relative degree associated with the state feedback exact linearization must be the same as the order of the system so that the nonlinear system is global linearized and has a satisfactory controller.

The purpose of the dynamic extension algorithm is to construct, starting with a system in which the relative degree $r = r_1 + r_2 \ldots + r_m$ is not equal to n, an extended (and feedback-modified) system in which the relative degree is possibly larger, and therefore-possibly after a number of iterations - equal to n.

It is possible to find two integers i_0, j_0, and make an element of $E(x)$ that is

$$a_{i_0j_0}(x^0) = L_{g_{j_0}} L_f^{r_{i_0}-1} h_{i_0}(x^0) \ne 0 \tag{51}$$

To define the dynamic feedback, in which $p(x)$ and $q(x)$ are arbitrary function satisfying $p(x^0) = 0$ and $q(x^0) = 1$.

$$\begin{aligned} &u_j = v_j, \quad j \ne j_0 \\ &u_{j_0} = \frac{1}{a_{i_0j_0}(x)}(p(x) + q(x)\xi - \sum_{\substack{j=1 \\ j \ne j0}}^{m} a_{i_0j}(x)v_j) \\ &\dot{\xi} = v_{j_0} \end{aligned} \tag{52}$$

The composition of Eqs. (39) and (52) define a new system that is

$$\begin{aligned} &\dot{x} = f(x) + \sum_{\substack{j=1 \\ j \ne j_0}}^{m} g_j(x)v_j + \frac{g_j(x)}{a_{i_0j_0}(x)}(p(x) + q(x)\xi - \sum_{\substack{j=1 \\ j \ne j0}}^{m} a_{i_0j}(x)v_j) \\ &\dot{\xi} = v_{j_0} \\ &y_i = h(x), \quad i = 1, 2, \ldots, m \end{aligned} \tag{53}$$

By definition, the $r_{i0}{}^{\text{th}}$ derivative of y_{i0} can be expressed in the form

$$y_{i_0}^{(r_{i_0})} = L_f^{r_{i_0}} h_{i_0}(x) + \sum_{j=1}^{m} a_{i_0j}(x)u_j \tag{54}$$

Thus, choosing $p(x) = -L_f^{r_{i_0}} h_{i_0}(x)$ and $q(x) = 1$ in the law yields, for the r_{i_0}th derivative of y_{i_0}, the simple expression

$$y_{i_0}^{(r_{i_0})} = \xi \tag{55}$$

The latter in turn yields

$$y_{i_0}^{(r_{i_0}+1)} = v_{j0} \tag{56}$$

Therefore, in the composed system Eq. (53), the lowest derivative of y_{i_0} which explicitly depends on the input is precisely the $(r_{i_0} + 1)$th derivative.

Suppose the dynamic extension algorithm has been iterated k times. Let

$$\begin{aligned} &\dot{x} = f(x) + g(x)[H(x, \xi) + K(x, \xi)\tilde{v}] \\ &\dot{\xi} = F(x, \xi) + G(x, \xi)\tilde{v} \\ &\tilde{v} = \tilde{\alpha}(x, \xi) + \tilde{\beta}(x, \xi)v \\ &y = h(x) \end{aligned} \tag{57}$$

with $\xi \in R^k$, denote the composition of the kth feedback laws of the form constructed at each stage of the algorithm.

After iterating k times of the dynamic extension algorithm, the relative degree r is equal to n. Therefore, there is no internal dynamic problem, and the nonlinear system becomes global linearized via the state feedback exact linearization.

4. Nonlinear robust control of PEMFC

In this section, a MIMO dynamic nonlinear model of PEMFC is developed by Eqs. (1)–(38), and it is then used to design a nonlinear robust controller by adopting state feedback exact linearization in order to minimize the pressure deviation between the hydrogen and oxygen. The main purpose of keeping the difference of pressures in a certain small range is to avoid a detrimental degradation of the fuel cell voltage, because the fuel cell voltage is a function of the pressures, each pressure needs to be appropriately controlled, and the pressures have bigger impact on the performance of fuel cells than other parameters [9,13]. In addition, keeping the small difference of pressures is also to protect the membrane from damage, and therefore, prolong the fuel cell stack life. In this paper, a pressure-control optimization algorithm is focused on developing for the PEMFC system. The stack current is considered as a disturbance to the system instead of an external input.

4.1. The state-space MIMO dynamic model

Consider the following MIMO nonlinear system with a disturbance:

$$\begin{aligned} \dot{x} &= f(x) + \sum_{i=1}^{m} g_i(x)u_i + L(x)w \\ y_i &= h_i(x), \quad i = 1, \ldots 2, m \end{aligned} \tag{58}$$

where $x \subset R^n$ is the state vector, $U \subset R^m$ is the input vector, $y \subset R^m$ is the output vector, and $f(x)$ and $g(x)$ are n-dimensional smooth vector fields. The w represents the disturbance variables, and $L(x)$ the dimensional vector field directly related to the disturbance.

According to Eqs. (1)–(38), the state-space MIMO nonlinear dynamic system model of PEMFC is expressed as follows:

$$\begin{aligned} \dot{x} &= f(x) + g_1(x)u_1 + g_2(x)u_2 + L(x)w \\ \begin{bmatrix} y_1 \\ y_2 \end{bmatrix} &= \begin{bmatrix} x_1 \\ x_3 \end{bmatrix} = \begin{bmatrix} h_1(x) \\ h_2(x) \end{bmatrix} \end{aligned} \tag{59}$$

where

$$\begin{bmatrix} x_1 \\ x_2 \\ x_3 \\ x_4 \\ x_5 \end{bmatrix} = \begin{bmatrix} P_{H_2} \\ P_{w,an} \\ P_{O_2} \\ P_{N_2} \\ P_{w,ca} \end{bmatrix}, \quad \begin{bmatrix} u_1 \\ u_2 \end{bmatrix} = \begin{bmatrix} u_a \\ u_c \end{bmatrix},$$

$$\begin{bmatrix} y_1 \\ y_2 \end{bmatrix} = \begin{bmatrix} P_{H_2} \\ P_{O_2} \end{bmatrix}, \quad w = i_m, \quad f(x) = 0$$

$$g_1(x) = RTs_{H_2} \begin{bmatrix} \dfrac{Y_{H_2}k_a}{V_a} - \dfrac{k_a}{V_a}\dfrac{x_1}{x_1+x_2} \\ \dfrac{\varphi_a P_v k_a}{V_a(x_1+x_2-\varphi_a P_v)} - \dfrac{k_a}{V_a}\dfrac{x_1}{x_1+x_2} \\ 0 \\ 0 \\ 0 \end{bmatrix},$$

$$g_2(x) = RTs_{air} \begin{bmatrix} 0 \\ 0 \\ \dfrac{Y_{O_2}k_c}{V_c} - \dfrac{k_c}{V_c}\dfrac{x_3}{x_3+x_4+x_5} \\ \dfrac{Y_{N_2}k_c}{V_c} - \dfrac{k_c}{V_c}\dfrac{x_4}{x_3+x_4+x_5} \\ \dfrac{\varphi_c P_v k_c}{V_c(x_3+x_4+x_5-\varphi_c P_v)} - \dfrac{k_c}{V_c}\dfrac{x_5}{x_3+x_4+x_5} \end{bmatrix}$$

$$L(x) = RT \begin{bmatrix} -\dfrac{Q_1}{V_a} + \dfrac{Q_1 x_1}{V_a(x_1+x_2)} \\ \dfrac{Q_2 x_2}{V_a(x_1+x_2)} - \dfrac{Q_2}{V_a} \\ -\dfrac{Q_1}{2V_c} + \dfrac{Q_1 x_3}{2V_c(x_3+x_4+x_5)} \\ 0 \\ \dfrac{Q_1}{V_c} - \dfrac{Q_1 x_5}{V_c(x_3+x_4+x_5)} - \dfrac{Q_2 x_5}{V_c(x_3+x_4+x_5)} + \dfrac{Q_2}{V_c} \end{bmatrix}$$

Eq. (59) implies that the input–output behavior of the PEMFC system is nonlinear and coupled. Each control variable u shows up after the first derivative of each $y_1 = x_1$ and $y_2 = x_3$, the relative degree vector $\{r_1, r_2\}$ is $\{1, 1\}$, so $r = r_1 + r_2 = 2 < 5$, and the decoupling matrix $E(x)$ is defined as

$$E(x) = \begin{bmatrix} L_{g_1}h_1(x) & L_{g_2}h_1(x) \\ L_{g_1}h_2(x) & L_{g_1}h_2(x) \end{bmatrix} \tag{60}$$

In order to achieve the control objective, three steps need to follow.

(1) Applying the dynamic extension algorithm, an extended system in which the relative degree r is equal to 5 after a number of iterations is achieved such that the internal dynamics problem is avoided.
(2) Using a nonlinear coordinate transformation in the state-space, there exists by a nonlinear static feedback such that the closed-loop system can be changed into Brunovsky canonical form in which the system is linear and controllable.
(3) Obtaining a nonlinear robust control law that not only can compensate nonlinearities but also can decouple and linearize the input and output behaviors.

According to Eq. (57), after iterating three times of the dynamic extension algorithm, the extended system is as follows,

$$\begin{aligned} \dot{\tilde{x}} &= \begin{bmatrix} \dot{x} \\ \dot{\xi}_1 \\ \dot{\xi}_2 \\ \dot{\xi}_3 \end{bmatrix} = \tilde{f}(x) + \tilde{g}_1(x)v_1 + \tilde{g}_2(x)v_2 + L(x)w \\ \begin{bmatrix} y_1 \\ y_2 \end{bmatrix} &= \begin{bmatrix} x_1 \\ x_3 \end{bmatrix} = \begin{bmatrix} h_1(x) \\ h_2(x) \end{bmatrix} \end{aligned} \tag{61}$$

where

$$\tilde{f}(x) = \begin{bmatrix} \xi_1 \\ \dfrac{g_{12}}{g_{11}}\xi_1 \\ \xi_3 \\ \dfrac{g_{24}}{g_{23}}\xi_3 \\ \dfrac{g_{25}}{g_{23}}\xi_1 \\ \xi_2 \\ 0 \\ 0 \end{bmatrix}, \tilde{g}_1(x) = \begin{bmatrix} 0 \\ 0 \\ \vdots \\ 1 \\ 0 \end{bmatrix}, \tilde{g}_2(x) = \begin{bmatrix} 0 \\ 0 \\ \vdots \\ 0 \\ 1 \end{bmatrix} \tag{62}$$

After the iteration, the relative degree vector r' is equal to 5. Then the decoupling matrix $E'(x)$ and the nonlinear control law are defined as

$$E'(x) = \begin{bmatrix} L_{g_1}L_f^2 h_1(x) & L_{g_2}L_f^2 h_1(x) \\ L_{g_1}L_f h_2(x) & L_{g_1}L_f h_2(x) \end{bmatrix} \tag{62}$$

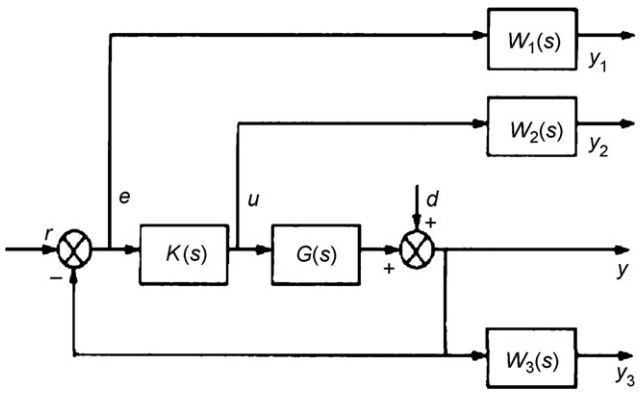

Fig. 2. Structure of mixed sensitivity problem.

$$\begin{bmatrix} u_1 \\ u_2 \end{bmatrix} = \begin{bmatrix} (1/a_{11}(x))(p_1(x) + q_1(x)\int(1/a'_{11}(x))\int v_1) \\ (1/a_{22}(x))(p_2(x) + q_2(x)\int v_2) \end{bmatrix} - E^{-1}(x)\begin{bmatrix} L_{11}(x) \\ L_{13}(x) \end{bmatrix} w \tag{63}$$

Therefore, there is no internal dynamic problem, and the nonlinear system becomes global linearized via the state feedback exact linearization. The nonlinear coordinate transformation in the state-space

$$z^1 = \begin{bmatrix} \phi_1^1(x) \\ \phi_2^1(x) \\ \phi_3^1(x) \end{bmatrix} = \begin{bmatrix} x_1 \\ \xi_1 \\ \xi_2 \end{bmatrix} z^2 = \begin{bmatrix} \phi_1^2(x) \\ \phi_2^2(x) \end{bmatrix} = \begin{bmatrix} x_3 \\ \xi_3 \end{bmatrix} \tag{64}$$

Then the Brunovsky canonical form is obtained

$$\begin{aligned} \dot{z}^1 &= A_1\begin{bmatrix} z_1^1 \\ z_2^1 \\ z_3^1 \end{bmatrix} + B_1 v_1 \quad y_1 = C_1\begin{bmatrix} z_1^1 \\ z_2^1 \\ z_3^1 \end{bmatrix} \\ \dot{z}^2 &= A_1\begin{bmatrix} z_1^2 \\ z_2^2 \end{bmatrix} + B_2 v_2 \quad y_2 = C_2\begin{bmatrix} z_1^2 \\ z_2^2 \end{bmatrix} \end{aligned} \tag{65}$$

with

$$A_1 = \begin{bmatrix} 0 & 1 & 0 \\ 0 & 0 & 1 \\ 0 & 0 & 0 \end{bmatrix}, \quad B_1 = \begin{bmatrix} 0 \\ 0 \\ 1 \end{bmatrix}, \quad C_1 = \begin{bmatrix} 1 \\ 0 \\ 0 \end{bmatrix}^{\mathrm{T}}$$
$$A_2 = \begin{bmatrix} 0 & 1 \\ 0 & 0 \end{bmatrix}, \quad B_2 = \begin{bmatrix} 0 \\ 1 \end{bmatrix}, \quad C_2 = \begin{bmatrix} 1 \\ 0 \end{bmatrix}^{\mathrm{T}}$$

4.2. H_∞ robust optimal control

To begin with, consider a standard mixed sensitivity problem [20] shown in Fig. 2. Where r, e, u, d and y are the reference input signal, the tracking error signal, the control input signal, the disturbance signal and the feedback output signal, respectively. $K(s)$ is the controller, and $G(s)$ the plant. y_1, y_2, y_3 is the weighting estimate signal of generalized plant.

Using the frequency-dependent weighting functions $W_1(s)$, $W_2(s)$ and $W_3(s)$ to weight the signals e, u and y respectively, a generalized system is constructed, which can be furthermore converted into the standard small gain problem. The H_∞ mixed sensitivity design problem is to find a proper rational controller that stabilizes the closed-loop system and satisfies [20]:

$$\min\left\|\Phi\right\|_\infty = \left\|\begin{matrix} W_1 S \\ W_2 R \\ W_3 T \end{matrix}\right\|_\infty = \gamma \tag{66}$$

where γ is the optimal H_∞ norm, $W_1(s)$, $W_2(s)$ and $W_3(s)$ are weighting functions for the sensitivity matrix function S(s), the control signal sensitivity matrix R(s), and the complementary sensitivity matrix function $T(s)$, respectively, are expressed as:

$$\begin{aligned} S &= (I + GK)^{-1} \\ R &= K(I + GK)^{-1} = KS \\ T &= GK(I + GK)^{-1} = I - S \end{aligned} \tag{67}$$

For $W_1(s)$ and $W_3(s)$, they need to satisfy the inequality constraint:

$$\sigma[{W_1}^{-1}(jw)] + \sigma[{W_3}^{-1}(\mathrm{j}w)] \geq 1 \tag{68}$$

As it is known, the sensitivity function is especially interesting from the control point of view as it has properties that characterize both the quality and the speed of the closed-loop temporal response. Bearing in mind that $W_1(s)$ must weight the sensitivity function, its design is proposed to be a diagonal matrix of transfer functions. And each diagonal element of $W_1(s)$ must be designed bearing in mind that its inverse should shape to the each diagonal element of S(s) as an upper bound. The inverse of $W_1(s)$ must be stable, minimum phase and the maximum singular value of $\gamma{W_1}^{-1}(s)$ must greater than the maximum singular value of S(s) for overall frequency range:

$$\sigma[S(jw)] < \sigma[\gamma{W_1}^{-1}(\mathrm{j}w)] \tag{69}$$

Since the class of uncertainty employed corresponds to the multiplicative output one, $W_3(s)$ associate robust stability condition and the maximum singular value of $\gamma{W_3}^{-1}(s)$ must greater than the maximum singular value of T(s) for overall frequency range:

$$\sigma[T(jw)] < \sigma[\gamma{W_3}^{-1}(\mathrm{j}w)] \tag{70}$$

Moreover, taking into account that $W_3(s)$ must weight to the complementary sensitivity function, it is desirable that the module of $W_3(s)$ has a high value in order to impose that T(s) has a small gain at high frequencies.

$W_2(s)$ is usually taken as diagonal constant matrix to avoid increasing the order of the controller.

According to the requirements on the robustness and performance of the PEMFC system which is mentioned above, the structures of W_{11}, W_{12}, W_{13}, W_{21}, W_{22}, W_{23} are selected:

$$\begin{aligned} W_{11}(s) &= \frac{42.3 \times (s + 106.8)}{(s + 0.0012)^2} \\ W_{12}(s) &= 0.0000188 \\ W_{13}(s) &= 0.005(s + 13.9) \\ W_{21}(s) &= \frac{118.3 \times (s + 60.8)}{(s + 1.15)^2} \\ W_{22}(s) &= 0.00021 \\ W_{23}(s) &= 0.002(s + 10.6) \end{aligned} \tag{71}$$

Meanwhile, the H_∞ mixed sensitivity problem could be tackled based on solving 2-Riccati Eq. (19). Then the optimal H_∞ controllers for inlet flow rates of anode and cathode which norm γ_1 and γ_2 are

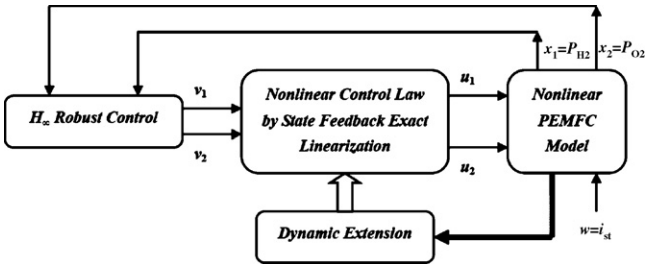

Fig. 3. Overall control scheme of PEMFC system.

0.85 and 0.58 are obtained:

$$K_1(s) = \frac{2.8 \times 10^6 (s+0.46)(s+43.7)(s+2.2)(s+1.9)}{(s+3.2\times 10^4)(s+0.001)(s+0.06)(s+101.3)(s+60.4)}$$

$$K_2(s) = \frac{11.2 \times 10^5 (s+46.9)(s+0.01)(s+0.2)}{(s+2.384)(s+1.9\times 10^4)(s+2.4)(s+1.9)} \quad (72)$$

Therefore, according to Eq. (61), the outputs P_{H_2} and P_{O_2} track asymptotically the desired trajectory 3 atm by adding the optimal H_∞ controllers mentioned in [34,35]. As shown in Fig. 3, the main objective of this control scheme is to design a nonlinear robust controller by appropriately defining a transformation mapping scheme that transforms the original nonlinear system into a linear and controllable closed-loop system.

5. Experimental

The PEMFC test system was set up in the Fuel Cell Application Centre (FAC), Temasek Polytechnic Engineering School.

5.1. The Cell/Stack

In this experiment, a 20-cell stack, which was designed and fabricated by Singapore GasHub and the FAC, as shown in Fig. 4, was tested for the validation of simulation results. A Nafion 112 membrane was used as the electrolyte, the Pt loading on electrodes is 0.4 mg cm^{-2} in the catalyst layer, graphite foil with serpentine flow channel was used as the bipolar plate, and the active area of the electrode is 150 cm^2 for the stack [36,37].

5.2. Steady-state polarization measurement

For the steady-state polarization measurement, both the hydrogen and air are humidified before entering the fuel cell stack. The air is humidified to 100% by using EFH-100WA solid-state humidifier from EnerFuel, Inc., while a hydrogen recycling pump is used to achieve the self-humidification of hydrogen at the anode, as presented in Fig. 5. The stack temperature is 323 K, the pressure of both sides is 0.5 atm, and the fuel cell stack repeatedly runs under full load to achieve stable performance before the steady-state polarization measurements are carried out.

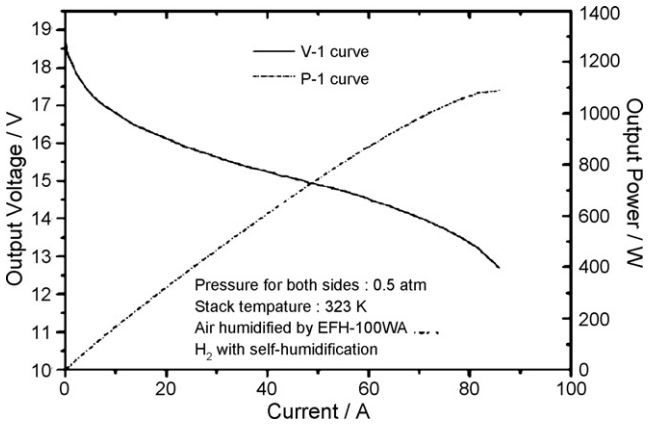

Fig. 5. Polarization and power curve of the experimental PEMFC stack.

5.3. Transient response measurement

To study the transient response of the fuel cell, two items would be clarified: cold start and hot start. In this experiment, cold start means that the hydrogen goes to the ON/OFF valve only at the moment the system starts and hot start means that the hydrogen always fully fills up the cell/stack even when the system does not work. The advantage of cold start is that the gas is confined within the pipe when the system is in standby, and is more reliable and safe; the disadvantage is that it will affect the lag time of the system. The advantage of hot start is that the starting of the system is swift and the lag of the system can be shortened effectively; the disadvantage is that the fuel stays inside the cell/stack, and some reaction and crossover between the MEA will take place; meanwhile, there will be leakage of the fuel, and thus, the system fabrication must be designed in a special way. If a small-capacity battery or an ultra-capacitor is employed in the output port of the fuel cell, the disadvantage of the cold start can be compensated, and it is accepted by the user mostly for its safety. Thus, we focus on the cold start in this study.

5.4. The Equipments

The voltage response, the voltage versus current curve, and the resistance of the cell/stack are measured by Scribner Associates 890 CL and LeCroy Waverunner LT344. The mass flow controllers with electromagnetic valves are installed to control the hydrogen flow and air flow to record the response of the output voltage and minimize the delay of the gas pipe. The humidifiers are used to prevent dehydration of the fuel cell membrane and improve the reaction rate. A hydrogen purge system including segregators is applied to increase the utility of fuel. The water cooling system used is Julabo FP40, which uses PID algorithm to control the temperature and has a resolution of 0.1 °C. Fig. 6 shows the diagram of the PEMFC test system.

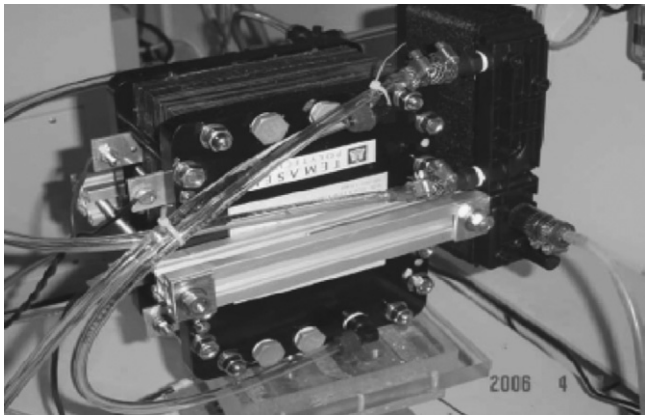

Fig. 4. Experimental PEMFC Stack.

6. Model validation and simulation results

In this paper, the Matlab/Simulink is used to setup the PEMFC system dynamic model with nonlinear robust controller. To verify

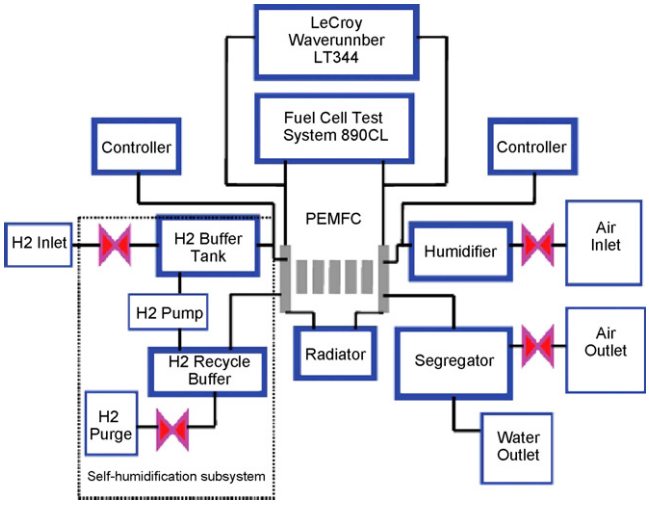

Fig. 6. Diagram of the PEMFC test system.

the validity of model, an experimental of a 1 kW PEMFC stack with 20 cells was conducted. The performances of the stack, such as output voltage versus current (V–I) curve and power versus current (P–I) curve, are presented in Fig. 5. It can be seen that the stack can give a 1 kW output at about 70 A of current.

Fig. 7 shows the measurement results of the transient voltage and the simulating dynamic response curve when the load current changed from 0 A to 7.5 A, 15 A, 30 A and 52.5 A individually. The voltage curve went down gradually since the current dragged from the stack increased as the load increased; at any moment, more charges will move and accumulate on the charge double layer, which decrease the inner resistance of the PEMFC and, in turn, affects the dynamic response of the fuel cell. The comparison shows that the difference of the average output voltage is less than 0.2 V when the load increases to different values. Moreover, the difference between the measurement and the simulation gradually increases when the load increases, so it can be seen that the simulation dynamic curve totally agrees with the actual tested results, and that the model developed can be used to simulate the dynamic response of the actual PEMFC. Furthermore, it verifies the validity of the model developed and the simulation results.

To compare the efficiency of the proposed nonlinear robust controller (NRC), the nonlinear generic model control (GMC) approach [12,13,33] is also implemented for the PEMFC system. The dynamic response of the hydrogen pressure and oxygen pressure as the load current changed in step are shown in Figs. 8 and 9, where the load

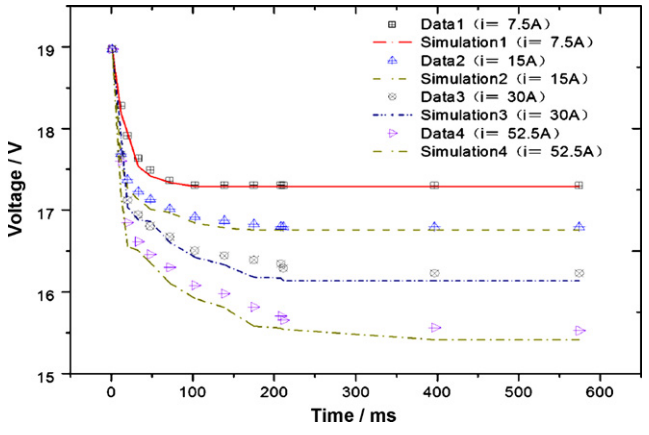

Fig. 7. Experimental results and simulation curves of transient voltage by increasing the load.

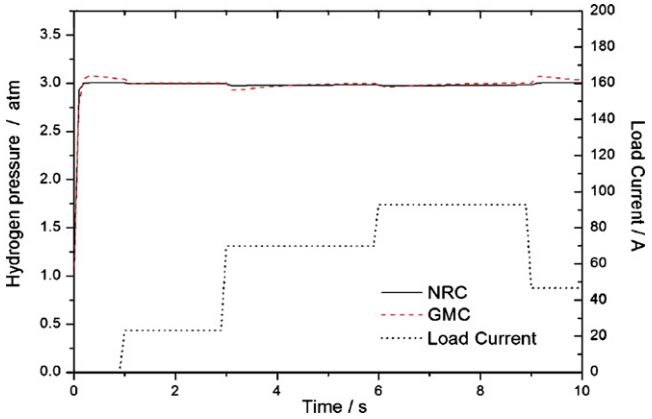

Fig. 8. Variation of hydrogen pressure.

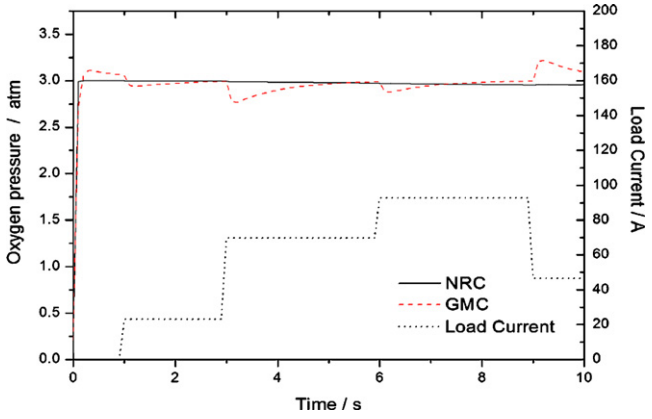

Fig. 9. Variation of oxygen pressure.

current is changed from 0 A to 92.8 A for simulating the accelerated and decelerated process of electrical vehicle. Fig. 10 displays the absolute value of the difference between the hydrogen and oxygen partial pressures. It is found in Fig. 10 that the NRC controller has a better transient response than the GMC controller. Generally, an increase in the load current causes a decrease in reactant pressures because more fuel consumption is required. However, the flow rates vary with the load current in the same way and compensate for the increased fuel consumption.

Figs. 11 and 12 give the dynamic responses of the hydrogen and the oxygen flow rates under the load current variations. It is observed that the oxygen flow rate has bigger variations than

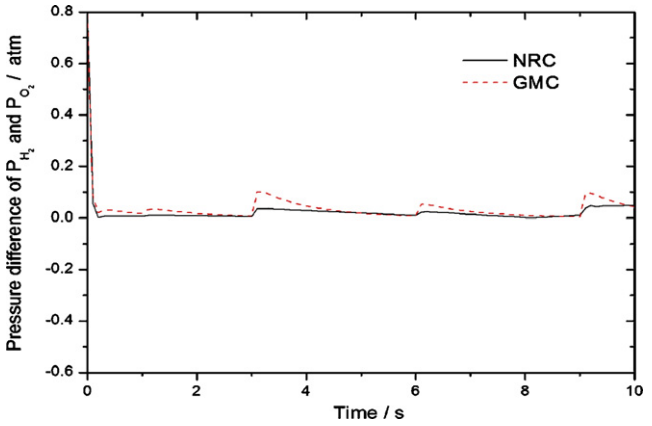

Fig. 10. Variation of pressure difference of hydrogen and oxygen.

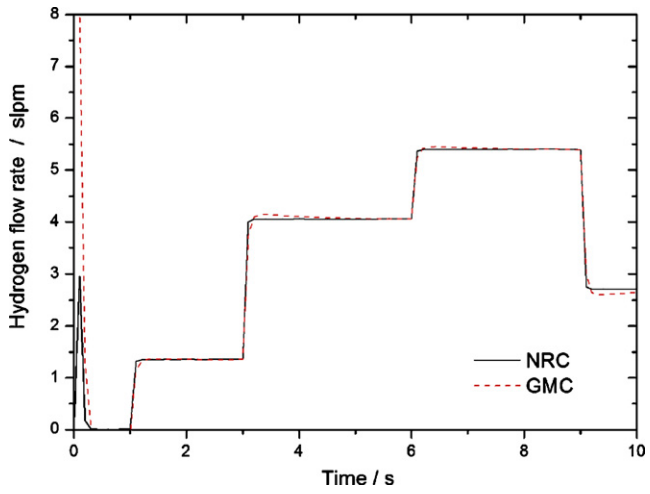

Fig. 11. Variation of hydrogen flow rate.

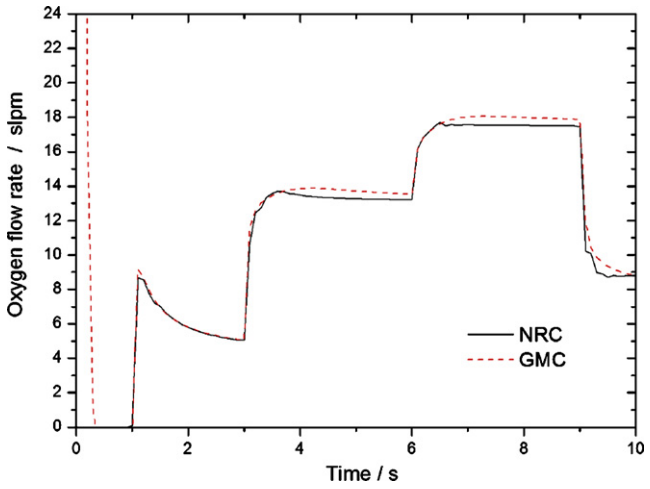

Fig. 12. Variation of oxygen flow rate.

hydrogen because the oxygen flow rate is more sensitive to the load current variation than the hydrogen flow rate.

Figs. 13–15 show that the NRC controller is more stable than the GMC controller under the load current variations for the states $P_{v,an}$, $P_{v,ca}$, and P_{N_2}. Therefore, the internal dynamics problem of the nonlinear robust controller is avoided, because applying the state feedback exact linearization with the dynamic extension algorithm can make the relative degrees have the same order of the system so that the nonlinear system is global linearized and has a satisfactory controller, that is not achieved in [12,13].

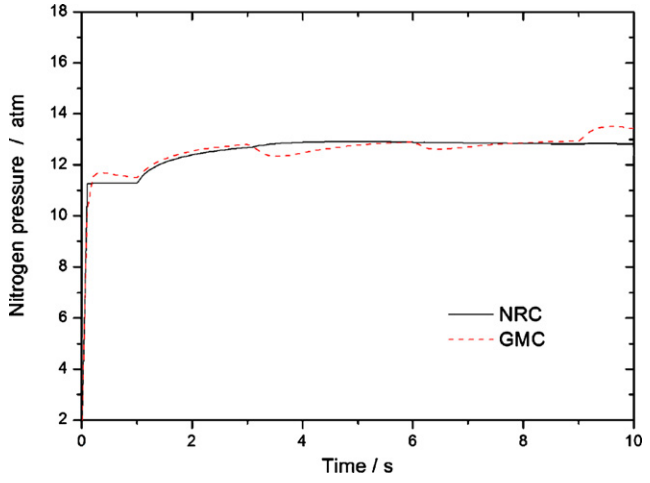

Fig. 13. Variation of nitrogen pressure.

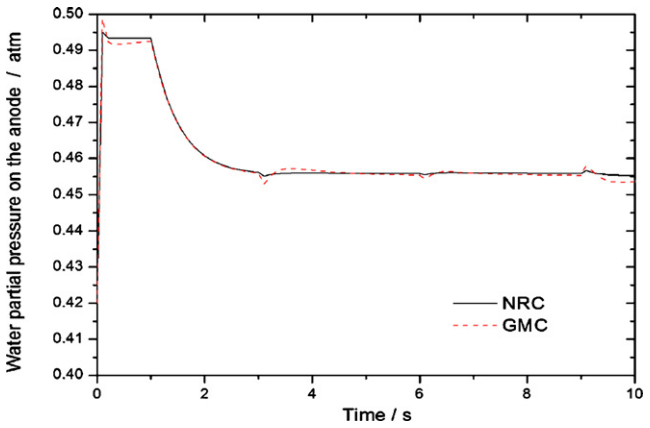

Fig. 14. Variation of water partial pressure on the anode.

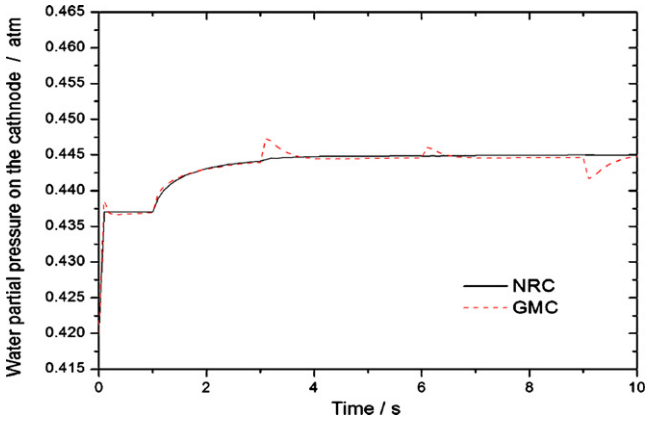

Fig. 15. Variation of water partial pressure on the cathode.

7. Conclusions

In this paper, a MIMO nonlinear dynamic model of PEMFC which is implemented in Matlab/Simulink environment is proposed for designing a nonlinear robust control by the state feedback exact linearization with the dynamic extension algorithm. By adding H_∞ robust control to the state feedback control law, the steady-state error due to parameter uncertainty can be reduced and the system is guaranteed to have better robustness. The comparison between the experimental data and simulation results shows that the model developed is validity and operable. The simulation results demonstrate that the nonlinear robust controller has better transient responses to guarantee stable operation of the system when the vehicle running process is simulated. Therefore, the proposed nonlinear robust control strategy should be extended to the design of an overall control scheme for PEMFC system and should be prolonged the operational life of PEMFC.

References

[1] J. Larminie, A. Dicks, Fuel Cell Systems Explained, Wiley, NewYork, 2002.
[2] C. Wang, M.H. Nehrir, IEEE Trans. Energy Convers. 22 (December (4)) (2007) 864–872.
[3] C. Wang, M.H. Nehrir, H. Gao, IEEE Trans. Energy Convers. 21 (June (2)) (2006) 586–595.

[4] A. Vahidia, A. Stefanpoulou, H. Peng, Model predictive control for starvation prevention in hybrid fuel cell system, in: Proceedings of the American Control Conference, 2004, pp. 834–839.
[5] J. Golbert, R. Lewind, J. Power Sources 135 (2) (2004) 135–151.
[6] R. Yuan, G.Y. Cao, X.J. Zhu, Predictive control of proton exchange membrane fuel cell (PEMFC) based on support vector regression machine, in: 2005 International Conference on Machine Learning and Cybernetics, 2005, pp. 4028–4031.
[7] J.O. Schumacher, P. Gemmar, M. Denne, et al., J. Power Sources 129 (1) (2004) 143–151.
[8] P.E. Almeda, G. Smoesm, IEEE Trans. Ind. Appl. 41 (1) (2005) 237–245.
[9] J. Purkrushpan, A.G. Stefanopoulou, H. Peng, IEEE Control Syst. Mag. 24 (April (2)) (2004) 30–46.
[10] J. Purkrushpan, H. Peng, Control of Fuel Cell Power Systems: Principle, Modeling, Analysis and Feedback Design, Springer–Verlag, Berlin, Germany, 2004.
[11] L.-Y. Chiu, B. Diong, R.S. Gemmen, IEEE Trans. Ind. Appl. 40 (July (4)) (2004) 970–977.
[12] W.K. Na, B. Gou, B. Diong, IEEE Trans. Ind. Appl. 43 (November (6)) (2007) 1426–1433.
[13] W.K. Na, B. Gou, IEEE Trans. Energ. Convers. 23 (March (1)) (2008) 179–190.
[14] J.J.E. Slotine, W. Li, Applied Nonlinear Control. Englewood Cliffs, Prentice-Hall, NJ, 1991.
[15] A. Isidori, Nonlinear Control Systems, 3rd ed., Springer–Verlag, London, U.K., 1995.
[16] Q. Li, Y. Sun, S. Mei, Nonlinear Control Systems and Power System Dynamics, Kluwer, Norwell, MA, 2001.
[17] B.W. Bequette, Ind. Eng. Chem. 30 (1991) 1391–1413.
[18] Y.S. Hung, B. Pokrud, IEEE Trans. Automatic Control 37 (6) (1992) 820–824.
[19] C.D. Yang, H.C. Tai, C.C. Lee, J. Dyn. Sys., Meas. Control 119 (1) (1997) 101–105.
[20] A.K. Christiansson, B. Lennartson, Weight selection for H_∞ using genetic algorithms, in: Proceedings of the 14th World Congress of IFAC, Beijing, 1999, pp. 25–30.
[21] M.D. Lukas, K.Y. Lee, H. Ghezel-Ayagh, IEEE Trans. Energ. Convers. September (16) (2001) 289–295.
[22] J.M. Correa, F.A. Farret, L.N. Canha, An analysis of the dynamic performance of proton exchange membrane fuel cells using an electrochemical model, in Industrial Electronics Society, 2001. IECON'01. The 27th Annual Conference of the IEEE, November 29–December 2 2001, vol. 1, pp. 1147–1150.
[23] Kourosh Sedghisigarchi, Ali Feliachi, IEEE Trans. Energ. Convers. June (19) (2004) 423–428.
[24] J.C. Amphlett, M. Baumertr, F. Mannr, J. Electrochem. Soc. 142 (January (1)) (1995) 9–15.
[25] J. Kim, M. Lees, S. Srinivasan, J. Electrochem. Soc. 142 (August (8)) (1995) 2670–2674.
[26] J.C. Amphlett, R.F. Mann, B.A. Peppley, P.R. Roberge, A. Rodrigues, J. Power Sources 61 (July–August (1–2)) (1996) 183–188.
[27] R.F. Mann, J.C. Amphlett, M.A. Hooper, et al., J. Power Sources 80 (March (1–2)) (2000) 173–180.
[28] R. Andrew, X.G. Li, J. Power Sources 102 (December (1–2)) (2001) 82–96.
[29] M.J. Khan, M.T. Labal, Fuel Cells 5 (1) (2005) 97–104.
[30] C. Wang, M.H. Nehrir, Steven R. Shaw, IEEE Trans. Energ. Convers. 20 (June (2)) (2005) 442–451.
[31] M.J. Khan, M.T. Labal, Fuel cells 5 (April (4)) (2005) 463–475.
[32] P.R. Pathapati, X. Xue, J. Tang, J. Renew. Energ. 30 (January (1)) (2005) 1–22.
[33] M.A. Henson, D.E. Seborg, J. Proc. Control May (1) (1991) 122–139.
[34] J. Sun, V. Kolmannovsky, IEEE Trans. Control Syst. Technol. 3 (November (6)) (2005) 911–913.
[35] M. Serra, J. Auado, X. Ansede, J. Riera, J. Power Sources 151 (2005) 93–102.
[36] S. Giddey, F.T. Ciacchi, S.P.S. Badwal, J. Power Sources 125 (January (2)) (2004) 155–165.
[37] M. Han, S.H. Chan, S.P. Jiang, J. Power Sources 159 (September (2)) (2006) 1005–1014.